Kinetics of laser irradiated nanoparticles cloud

S. K. Mishra, M. Upadhyay Kahaly, and Shikha Misra

Citation: Physics of Plasmas **25**, 023703 (2018); doi: 10.1063/1.5016916
View online: https://doi.org/10.1063/1.5016916
View Table of Contents: http://aip.scitation.org/toc/php/25/2
Published by the American Institute of Physics

Kinetics of laser irradiated nanoparticles cloud

S. K. Mishra,[1,a)] M. Upadhyay Kahaly,[1] and Shikha Misra[2]
[1]Extreme Light Infrastructure-Attosecond Light Pulse Source (ELI-ALPS), Szeged 6720, Hungary
[2]F-32, CSIR-CEERI, Col., Pilani 333031, India

(Received 22 November 2017; accepted 23 January 2018; published online 5 February 2018)

A comprehensive kinetic model describing the complex kinetics of a laser irradiated nanoparticle ensemble has been developed. The absorbed laser radiation here serves dual purpose, viz., photoenhanced thermionic emission via rise in its temperature and direct photoemission of electrons. On the basis of mean charge theory along with the equations for particle (electron) and energy flux balance over the nanoparticles, the transient processes of charge/temperature evolution over its surface and mass diminution on account of the sublimation (phase change) process have been elucidated. Using this formulation phenomenon of nanoparticle charging, its temperature rise to the sublimation point, mass ablation, and cloud disintegration have been investigated; afterwards, typical timescales of disintegration, sublimation and complete evaporation in reference to a graphite nanoparticle cloud (as an illustrative case) have been parametrically investigated. Based on a numerical analysis, an adequate parameter space describing the nanoparticle operation below the sublimation temperature, in terms of laser intensity, wavelength and nanoparticle material work function, has been identified. The cloud disintegration is found to be sensitive to the nanoparticle charging through photoemission; as a consequence, it illustrates that radiation operating below the photoemission threshold causes disintegration in the phase change state, while above the threshold, it occurs with the onset of surface heating. *Published by AIP Publishing.*
https://doi.org/10.1063/1.5016916

I. INTRODUCTION

Nanoparticle assembly has been the subject of extensive research activities for use of these unique structures in wide ranging applications.[1–6] Enormous scientific interest towards nanoparticle research originates from the fact that they are, in effect, a bridge between bulk materials and atomic/molecular structures. In such a small scale, due to the confinement of electronic states, while there was possible dangling of some atomic bonds at the nanoparticle surface, the properties of materials dramatically change as the surface to volume ratio of the material becomes significant;[2–4] for the bulk (larger than a few microns), the surface to volume scaling becomes insignificant. The intriguing and sometimes exotic properties of nanoparticles are, therefore, largely due to the large surface area of the material, which dominates the contribution. Nanoparticles often possess unexpected optical properties through electron confinement resulting in quantum effects. For instance, gold nanoparticles under the influence of nanosecond (ns) ultraviolet (UV) pulses are shown to liberate electrons predominantly through the thermionic emission via inter-band excitation.[7] In a recent analysis, a significant rise in the surface temperature[8] of gold nanoparticles indicating large thermionic current is reported. A wide variety of nanoparticles demonstrate[9] a scalable band gap for better absorption of photons along with significant energy transfer which allows the absorbed photon energy to be efficiently captured as heat by carriers. Thus, to tailor the electronic structures and tune electron emission assisted properties, a nanoparticle assembly is considered an appropriate system from numerous perspectives.

The analysis of laser irradiated nanoparticles is of essence in gas phase/aerosolized nanoparticle synthesis and characterization.[10] The characterization of soot-laden[11,12] and synthetic nano-aerosols[13–15] via laser induced incandescence (LII) diagnostics is a significant example where the nanoparticle ensemble is heated via a laser pulse to increase its temperature to incandescence for spectroscopic modelling and in defining the nanoparticle size, the particle volume ratio and other relevant physical features.[10] In another interesting perspective, laser assisted reshaping, fragmentation and assembly of a gold (Au) nanoparticle ensemble have been proposed by using pulses of ns-fs time scales[16] where relevant phases occur due to transient features of coexisting excitation (heating) and relaxation (cooling) phenomena. This scheme could be utilized in achieving monodisperse gold nano-spheres via pulse laser irradiation of polyhedral nanocrystal colloids (particularly suitable for medical applications) and in fabricating the nanostructures of preferred optical properties.[16] On account of radiation absorption, the nanoparticle heating process is primarily described by stages of (i) temperature rise and (ii) substrate evaporation/sublimation due to the phase change process.[17,18] The instant temperature/substance diminution of the nanoparticle heating process is characterized by equations for particle and energy flux balance over the nanoparticle surface;[17] subsequently, the thermionic emission from hot nanoparticles is anticipated to play a significant role in its cooling.[17–20] In addition, on account of photo-thermionic/photoelectric effects under laser irradiation, time dependent charge acquisition on the

a)Author to whom correspondence should be addressed: nishfeb@gmail.com

nanoparticle surface essentially influences the charge dependent cooling mechanisms.[17] Hence, the particle heating and its charging are transient and mutually interdependent processes which should be incorporated adequately in explaining the kinetic features of the laser irradiated nanoparticle cloud. Thus, contrary to earlier analyses[20,21] of a laser irradiated nanoparticle cloud, the present work includes the instantaneous charge dependence of the inherent physical mechanisms and the charging phenomenon of direct photoemission of electrons from irradiated nanoparticles in addition to typical thermionic emission. The transient evolution of positive charge[22] over the nanoparticles in the heating process leads to growing Coulomb repulsion between nanoparticles in the sample cloud which might overcome the inter-particle (weak van der Waals/ionic/covalent) bonding to disintegrate the ensemble.

In this analysis, a formalism describing the kinetics of a laser irradiated nanoparticle cloud characterizing the evolution of charge, temperature and size of the nanoparticles along with subsequent plasma density has been established; the formulation considers a uniformly irradiated ensemble of monodispersed nanoparticles, joined through van der Waals linkage and takes account of the mean charge theory.[23,24] In writing the dynamical equations for charge continuity, the surface temperature, mass ablation and population density/mean temperature of the resulting electron cloud, the processes of photoelectric/thermionic emission, charge desorption, electron accretion, sublimation and radiation cooling have been taken into account;[17] the instantaneous nanoparticle charge dependence of constituent mechanisms is an inherent feature and consistently accounted for throughout this analysis. For the sake of simplicity in analysis, nanoparticles are considered to be spherical in nature and assumed to retain their spherical shape in the evaporation (phase change) process. In addition, sputtering/fragmentation of the nanoparticles have also been ignored, which is a reasonable assumption as friction and mutual collisions in the environment are insignificant in comparison to the other physical processes considered herein. The significance of charge accumulation on nanoparticle cloud disintegration has also been investigated. The analytical formulation describing model equations of the problem has been established in Sec. II. Section III includes the expressions and significant parameters in relevance to the physical processes incorporated herein along with a computational scheme. The physical interpretation and discussion of the analytical/numerical results in reference to a graphite nanoparticle cloud (as an illustrative case) is given in Sec. IV on Numerical results and discussion. A summary of the outcome in Sec. V concludes the paper.

II. ANALYSIS

Consider a monochromatic laser of uniform radiation is probed to a monodispersed spherical nanoparticle assembly having number density n_d. In this process, a finite fraction (say α) of the incident flux, depending on the surface material and radiation properties, is absorbed; the absorbed photon (laser) energy triggers two mutual effects,[25] namely (i) rise in the nanoparticle surface temperature invoking thermionic emission of electrons and (ii) photoelectric emission of electrons through direct absorption of a photon by an electron. On account of electron emission and their consequent accretion over the surface, nanoparticles acquire a finite positive charge; the transient evolution of the mean charge over the nanoparticle surface (z_s) may be expressed as[23,24]

$$dz_s/dt = 4\pi a^2\left[(f_{th}+f_{ph}) - \eta_e f_{ec}\right] - f_s, \tag{1}$$

where f_{th} and f_{ph} infer the flux of electrons associated with thermionic and photoelectric emission from the nanoparticles, while f_{ec} corresponds to the electron flux accreting over its surface, f_s refers to the rate of charge desorption in the process of mass ablation[26] ($f_s = -2\dot{a}|z_s|/a$) and a is the instant nanoparticle radius; the expressions for $f's$ are depicted in Sec. III. For simplification, photoemission via multiphoton absorption is ignored, which requires the synchronization of complex processes of photon absorption and collisional energy dissipation.

The continuous laser absorption by the nanoparticle surface causes heating and effectively triggers a rise in the surface temperature; this results in fusion of the nanoparticle material[27] and may lead to mass sublimation. In addition, radiative cooling, photo/thermionic emission of electrons and electron accretion mechanisms also contribute to energy balance over nanoparticles. The balance of energy over the nanoparticles may thus be written as[18]

$$\begin{aligned}\left(m_s s\frac{dT_s}{dt}\right) = \varepsilon_{net} = 4\pi a^2[(\gamma/4)I_{abs} + \eta_e f_{ec}\varepsilon_{ec} \\ - \left[f_{th}(\varepsilon_{th}+\varphi) + f_{ph}\varepsilon_{ph}\right] - l_m f_{sub} \\ - \in \sigma(T_s^4 - T_o^4)],\end{aligned} \tag{2}$$

where $m_s = (4\pi/3)a^3\rho$ is the mass of the nanoparticle, ρ and s correspond to the bulk density and the specific heat of the nanoparticle material, T_s and T_o refer to the surface temperature of the nanoparticle and the surrounding environment (radiative) temperature, f_{sub} refers to the mass loss rate due to sublimation, $l_m = (L_m/\mu)$, where L_m is the latent heat of sublimation per mole and μ refers to gram molecular weight of the average sublimated molecule, ε_{th} (ε_{ph}) is the mean energy of thermionic (photoemitted) electrons on the nanoparticle surface, φ is the material work function, ε_{ec} corresponds to the mean energy of electrons accreting over the nanoparticle surface and $\in$ is thermal emissivity, while k and σ are the Boltzmann and the Stephan Boltzmann constants, respectively; the relevant expressions are listed in Sec. III.

The first two terms in the right hand side (rhs) parenthesis of Eq. (2) correspond to the net power gained by the nanoparticle on account of laser absorption and electron accretion over its surface. The third term refers to the energy loss per unit time per unit area due to thermionic and photoelectric emission, respectively. It may be stated here that energy loss per electron (and hence the cooling rate) is higher in thermionic emission than in the photoemission; this is primarily due to the fact that in the case of thermionic emission, the thermal energy is also consumed in

overcoming the threshold work function, while for photoemission, this threshold is overcome by photon energy. The next term is the net power loss per unit area from the nanoparticle surface due to sublimation of mass. The last term corresponds to the energy loss due to irradiation to the surrounding environment. In writing the above energy equation, the contribution of laser induced oxidation to the particle's energy balance equation is assumed to be insignificant. In addition, for simplicity, we have assumed that the thermal conductivity is large or the nanoparticle size is small enough so that the lattice temperature raises uniformly.[20] Due to the energy exchange between laser radiation and particles in the heating process, the surface temperature rises until it reaches the mass ablation (i.e., evaporation/sublimation) temperature. After attaining the sublimation (evaporation) temperature, all the energy received by nanoparticles is utilized in the process of phase change of the surface material. Assuming a uniform surface temperature over the nanoparticle volume and isotropic mass loss through sublimation/evaporation during phase change, the equation for change in the radius (or mass) can be expressed as[18]

$$l_m(dm_s/dt) = -\varepsilon_{net}. \tag{3a}$$

Substituting the instant mass in terms of material density and nanoparticle volume, the phase change equation reduces to

$$l_m\rho(da/dt) = -[(\gamma/4)I_{abs} + \eta_e f_{ec}\varepsilon_{ec} - [f_{th}(\varepsilon_{th}+\varphi) + f_{ph}\varepsilon_{ph}] - l_m f_{sub} - \in \sigma(T_s^4 - T_o^4)]. \tag{3b}$$

In the process of the laser irradiated nanoparticle cloud, the generation of electrons takes place on account of thermionic/photoelectric emission and mass sublimation, while electrons deplete on the nanoparticle surface due to their accretion. The net production rate of electrons can thus be given by[27]

$$(dn_e/dt) = 4\pi a^2 n_d\left[(\beta/m_n)f_{sub} + f_{th} + f_{ph} - \eta_e f_{ec}\right], \tag{4}$$

where β is the number of free electrons produced per vaporized material atom.

The first term in the rhs of the parenthesis of Eq. (4) infers the generation rate of electrons per unit area from the sublimated material of the nanoparticles under the influence of radiation. The next two terms (2nd and 3rd) in the equation refer to the rise in electron population density per unit area per unit time by thermionic and photoelectric emission. The last term corresponds to the loss in electron population density because of its accretion over the nanoparticle. Subsequently, the mean energy (temperature) associated with the emitted electron cloud may thus be written as[18]

$$\frac{d}{dt}\left(n_e\frac{3kT_e}{2}\right) = 4\pi a^2 n_d[(\beta/m_n)f_{sub}\varepsilon_{sub} + f_{th}\varepsilon_{th} + f_{ph}\varepsilon_{po} - \eta_e f_{ec}\varepsilon_{ec}]. \tag{5}$$

In the above equation, ε_{sub} refers to the mean energy of electrons liberated through sublimation, while rest of the terms infers the energy associated with the electron generation processes, in accordance with their prior definitions. The set of equations [Eqs. (1)–(5)] are general in nature and describe the kinetics of the laser irradiated nanoparticle cloud.

On account of inherent kinetic processes, the nanoparticle in the ensemble may acquire a dynamic positive charge; the transient evolution of positive potential over nanoparticles induces the Coulomb repulsion (U_{rep}) between nanoparticles within the ensemble which might overcome the weak van der Waals binding energy (U_V), i.e., when $U_{rep} \geq U_V$, resulting in the phenomenon of nanoparticle cloud disintegration.[20] The respective expressions for U_{rep} and U_V are stated in Sec. III.

III. RELEVANT EXPRESSIONS AND PARAMETERS

Consider a nanoparticle cloud (with a number density n_d) is illuminated by a monochromatic source of uniform radiation. A finite fraction (α) of the incident photon flux (effectively $I_{abs} = \alpha I_{in}$) interacts with $\kappa\Lambda$ fraction of the electrons hitting the top layer from the inside,[28] which is utilized for increasing the surface temperature and consequent emission of electrons; here, κ is the probability per unit time of absorption of an incident photon per unit area per unit time by an electron hitting normally the top layer from inside and Λ refers to the absorbed photon flux. Assuming that the γ fraction of the absorbed photon flux utilized in particle heating and rise in the surface temperature results in modification of the electron energy distribution inside the nanoparticles,[25,29] rest of the photon flux, i.e., the $(1-\gamma)$ fraction is consumed in direct electron emission via a photoelectric effect. The expressions describing the respective mechanism used in analytical modelling [Eqs. (1)–(5)] are as follows:[24] $f_{ph}(z_s - 1) = (\Lambda_\nu/4)[\chi(\varepsilon_\nu)/\Phi(\varsigma)][\Phi(\varsigma - z_s\alpha_s) + z_s\alpha_s ln(\varsigma - z_s\alpha_s)]$, $\varepsilon_{ph}(z_s-1) = kT_s$, $f_{th}(z_s-1) = (A_o/e)T_s^2(1+z_s\alpha_s)\exp[-(z_s\alpha_s+\varphi_s)]$, $\varepsilon_{th}(z_s-1) = [[(2+z_s\alpha_s)/(1+z_s\alpha_s)]+z_s\alpha_s]kT_s$, $f_{ec}(z_s) = (kT_e/2\pi m)^{1/2}(1+z_s\alpha_e)$, $\varepsilon_{ec}(z_s) = [[(2+z_s\alpha_e)/(1+z_s\alpha_e)]+z_s\alpha_e]kT_e$, $\varepsilon_{sub} = kT_s$, $\alpha_s = e^2/akT_s$, $\Lambda_\nu = I_{abs}/h\nu = (\lambda/hc)I_{abs}$, $\varsigma = (h\nu-\varphi)/kT_s$, $f_{sub} = (m_n/2\pi kT_s)^{1/2}p_{vap}$, where p_{vap} is the vapour pressure and may be given by Clausius-Clapeyron equation as $\log_{10}p_{vap} = a_m - b_m/T_s$, a_m and b_m are the material dependent constants,[30] while m_n is the average mass of a sublimated atom/molecule.

The spectral dependence of photoelectric efficiency (χ) has been incorporated through Draine's formulation,[24] viz., $\chi(h\nu) = \chi_m(1-\varphi/h\nu)$, where χ_m refers to the optimum efficacy; this relation is applicable for the photons of energy higher than the work function (photoemission threshold). Another crucial parameter is γ, a fraction of absorbed radiation which is utilized in the nanoparticle heating. Intuitively, this fraction γ can be evaluated as follows: the electron emission flux from an uncharged surface may be given by $\chi\Lambda$; assuming that rest of the photon flux is utilized in heating the electrons inside, the fraction γ in terms of photoelectric yield may intuitively be expressed as $\gamma = (1-\chi)$. This expression shows that for radiation with photon energy lower than the work function (φ), all the radiation energy is utilized in nanoparticle surface heating. In reference to the nanoparticle

cloud disintegration process, expressions for van der Waals and Coulomb repulsion energy may be expressed as[31]

$$U_V = (A_H/6)\left[\left[2a^2/(\zeta^2 - 4a^2)\right] + (2a^2/\zeta^2) + ln\left[(\zeta^2 - 4a^2)/\zeta^2\right]\right],$$
$$U_{rep} = z_s^2 e^2/\zeta,$$

where $\zeta = 2a + d$, d refers to the inter particle (van der Waals bond) distance and A_H is the material dependent Hamaker constant.[31] Assuming that the location of particles remains intact, $\zeta(=2a_o + d)$ may be treated as constant for a given particle size a_o and d. The aforementioned expressions suggest that the cloud disintegration may occur either due to significant charge evolution (operating below sublimation temperature) or particle size/mass reduction (during phase change/sublimation) when particle charge accumulation is not individually significant to overcome the van der Waals bonding.

The analysis presented herein takes the following nanoparticle parameters into account for the illustrative calculations: material work function (φ), nanoparticle radius (a_o), number density (n_d), absorption coefficient (α), specific heat (s), latent heat of sublimation (L_m) and mass density (ρ). The prime feature of the work is to analyze the response of various parameters (listed above) on a nanoparticle ensemble under laser assisted thermionic plus photoemission effects and its consequences on their sustainability (via cooling), charging and cloud disintegration. With this notion, a uniformly irradiated ensemble of homogeneously dispersed graphite nanoparticles[20] has been considered for the illustrative purpose. Important nanoparticle parameters significant for the emission processes, namely the work function[24–26] (φ) and the nanoparticle radius[20] (a_o) have been identified, in particular, (Figs. 3, 4 and 6; discussed next). Furthermore, as the analysis takes into account of the mean charge theory, while the energy equations are written in terms of particle surface area, the results for parameters a, T_s, and z_s and different time scales (τ_d, τ_s, τ_a) are equally valid for all the constituent nanoparticles in the cloud. The variation in n_d only affects the electron density [via Eq. (4)] in the cloud, which effectively increases with increasing n_d; a plausible value $n_d = 100\,\mathrm{cm}^{-3}$ has been chosen for the illustration purpose. In addition, the absorbed radiation of laser ($I_{abs} = \alpha\, I_L$) has been used as an input parameter for calculations; thus, α variation is also inherently taken into account. The other parameters L_m, s and ρ corresponding to graphite have been taken from Refs. 26 and 27; considering the energy equations [Eqs. (2) and (3)], qualitatively, the large values of these parameters infer a larger sustenance of the nanoparticles due to efficient heat capacitance/cooling effects. The coefficient of Clausius-Clapeyron relation, i.e., a_m and a_m, has been taken from Refs. 32 and 33. The numerical computation takes into account of the following set of data (typical graphite carbon, Refs. 20, 24–26, 32, and 33): $L_m = 8.724 \times 10^{12}\mathrm{erg/mol}$, $s = 0.72 \times 10^7\mathrm{erg/gK}$, $m_n = 12\mathrm{amu}$, $T_o = 300\mathrm{K}$, $T_{so} = 300\mathrm{K}$, $\mu = 12$, $n_d = 100$, $a_o = (10-50)\,\mathrm{nm}$, $\varphi = 4.6\,\mathrm{V}$, $\lambda = 200\,\mathrm{nm}$, $\chi_m = 1.0$, $I_{abs} = \alpha I_{in} = 10^8\,\mathrm{W/cm^2}$, $A_H = 2.9\,\mathrm{eV}$, $d = 0.7\,\mathrm{nm}$, $a_m = 13.922$ and $b_m = 37471.62\,\mathrm{K}$.

Using adequate expressions along with initial conditions, viz., $z_s = 0$, $a = a_o$, $T_s = T_{so}$, $n_e = n_{eo}$ and $T_e = T_{eo}$ at $t = 0$, Eqs. (1)–(5) have been solved simultaneously with the help of a Mathematica tool to obtain the temporal evolution of the irradiated nanoparticle features. In computations, we examine the effect of various nanomaterial and laser radiation parameters on the evolution of various physics parameters of the phenomena. The numerical results corresponding to laser irradiated graphite nanoparticles are graphically presented in figures and discussed in Sec. IV.

IV. NUMERICAL RESULTS AND DISCUSSION

For a numerical appreciation of the kinetic model and physics understanding of the constituent mechanisms, computations have been performed for a specific set of material properties (consistent with graphite) and parameters, as mentioned in Sec. III. The kinetics procures the phenomena of rise in temperature (due to radiation absorption) and charge (through thermionic/photoelectric emission) of the nanoparticle along with the phase change process. The Coulomb interaction between the nanoparticles within an ensemble may overcome van der Waals bonding between them (i.e., $U_{rep} \geq U_V$), and the cloud might disintegrate; this instant (τ_d) in calculations has been identified as the disintegration timescale. The instant of rise in the nanoparticle temperature due to radiation absorption up to sublimation (evaporation) temperature is considered as the timescale for sublimation (τ_s). After this, the phase change of the surface material elicits its mass ablation and reduction in the particle size; the instant when sublimation results in complete evaporation of the nanoparticle (radius equivalent to atomic scale, for instance 0.1 nm) has been characterized by timescale τ_a. The dependence of aforementioned characteristic timescales (viz., τ_d, τ_s and τ_a) along with transient evolution of the subsequent physical parameters has been identified as a function of irradiation (photon) flux for different values of radiation and material parameters, using numerical integration of the kinetic equations [Eqs. (1)–(5)].

As an illustrative case, the transient evolution of the physical features associated with the graphite nanoparticle cloud under the influence of monochromatic radiation ($\lambda \sim 200\,\mathrm{nm}$) of different intensities is displayed in Fig. 1. As soon as the radiation illuminates the nanoparticle cloud, temperature rise takes place due to energy kinetics [Fig. 1(a)], and consequent electron emission leads to nanoparticle charging [Fig. 1(b)]. As in this case, photon energy is higher than that of the material work function ($h\nu > \varphi$), the charging of nanoparticles takes place on account of both thermionic and photoelectric effects by consuming, respectively, γ and the $(1-\gamma)$ fraction of the incident radiation flux. In the beginning phase, when the nanoparticle temperature rises significantly higher than the environment, it acquires a quasi-static equilibrium below the sublimation point; in this process, a significant rise in the particle charge also leads to disintegration of the nanoparticle cloud in the beginning phase (i.e., during temperature rise). As soon as the nanoparticle acquires the sublimation temperature (around τ_s) and mass ablation (and size reduction) becomes effective, the

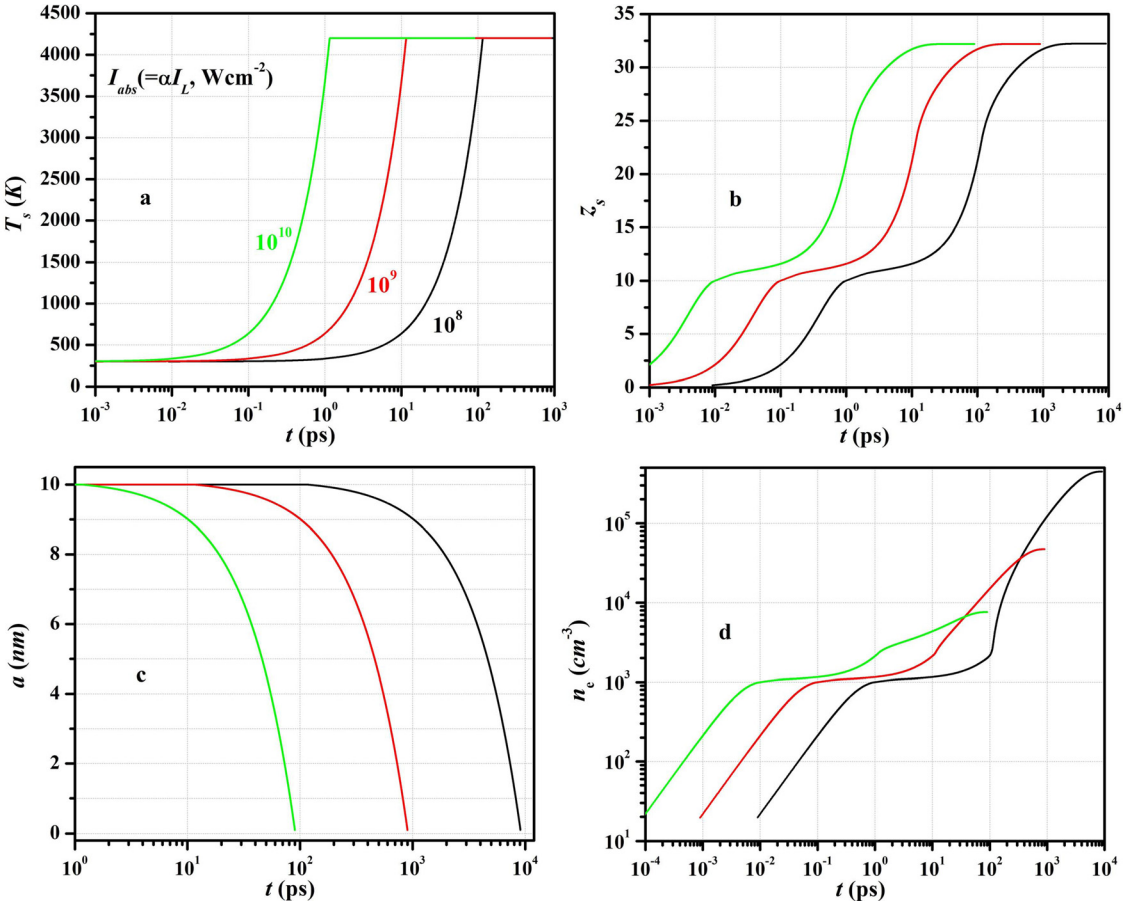

FIG. 1. Transient evolution of nanoparticle (a) temperature (T_s), (b) charge (z_s), (c) radius (a/a_o) and (d) ambient electron density (n_e) for an irradiated graphite nanoparticle cloud. The computations correspond to 200 nm wavelength radiation along with parameters stated in the text and the colour labels in the figure refer to different values of radiation flux (I_{abs}).

charging via mass desorption becomes significant and the nanoparticle charge rises sharply; the nanoparticle charge acquires an optimum magnitude and literally attains a quasi-steady state as the particle size approaches the atomic scale [Fig. 1(b)]. For instance, with radiation intensity $I_{abs}= 10^8$ W cm^{-2} and $a_o= 10$ nm, the disintegration occurs for $z_s \sim 5.8$ at $\tau_d \sim 0.31$ ps, while the sublimation of the surface material begins for $z_s \sim 23.1$ at $\tau_s \sim 115.4$ ps; the particle size reduces to an atomic scale ($\sim$0.1 nm) with $z_s \sim 32.2$ at $\tau_a \sim 9.1$ ns. The quicker (i.e., at a shorter timescale) rise in the nanoparticle charge [Fig. 1(b)] and temperature [Fig. 1(a)] with increasing radiation intensity displayed by the black ($I_{abs}= 10^8$ W cm^{-2}), red (10^9 W cm^{-2}) and green (10^{10} W cm^{-2}) color curves can be understood in terms of larger rate of energy absorption [Eq. (2)]. The transient evolution of nanoparticle size during phase change due to mass evaporation is illustrated in Fig. 1(c) which displays a sharp decay and a smaller timescale for the large radiation flux; this nature may be understood as a consequence of respective timescales of attaining sublimation temperature [at an instant τ_s, Fig. 1(a)] in order to initiate the phase change. The electron population generated in this process is illustrated in Fig. 1(d); the largest population density is obtained for the smaller radiation intensity which may be attributed to the sustenance of nanoparticles to a larger time span (τ_a) elucidating a higher possibility of generating electrons [via Eq. (4)]. The two humps (sharp variation) in this curve (for instance, at $\sim$0.3 ps and $\sim$115 ps for $I_{abs}= 10^8$ W cm^{-2}) apparently refer to the instants where the nanoparticle cloud disintegrates (τ_d) and sublimates (τ_s), respectively.

Figure 1 corresponds to a 200 nm wavelength radiation which is able to knockout the electron through direct photoemission from the Fermi level as the photon energy is sufficient enough to overcome the threshold barrier of graphite (i.e., 4.6 V work function). Next, we examine a case for 300 nm radiation flux which corresponds to photon energy $h\nu \sim 4.16\,\text{eV} < \varphi$ and prohibits the direct photoemission from nanoparticles; following Draine's formulation, this case infers that all the absorbed energy is thus utilized in system heating ($\gamma = 1$). In this case, the respective physical parameters in reference to Fig. 1 are displayed in Fig. 2. The surface temperature is noticed to rise faster in the case of 300 nm radiation [Fig. 2(a)] than that of Fig. 1(a); this behaviour may be attributed to the fact that all the energy absorbed is involved in temperature rise. In this course, the nanoparticle charge is primarily induced through thermionic emission (assisted by desorption during phase change) as illustrated in Fig. 2(b); in reference to Fig. 1(b), this figure also specifies the significance of direct photoemission in charging the irradiated nanoparticles. In simulation, in fact, it is observed that the disintegration occurs in the phase change regime ($>\tau_s$, evaporation phase) as the individual charge growth over the

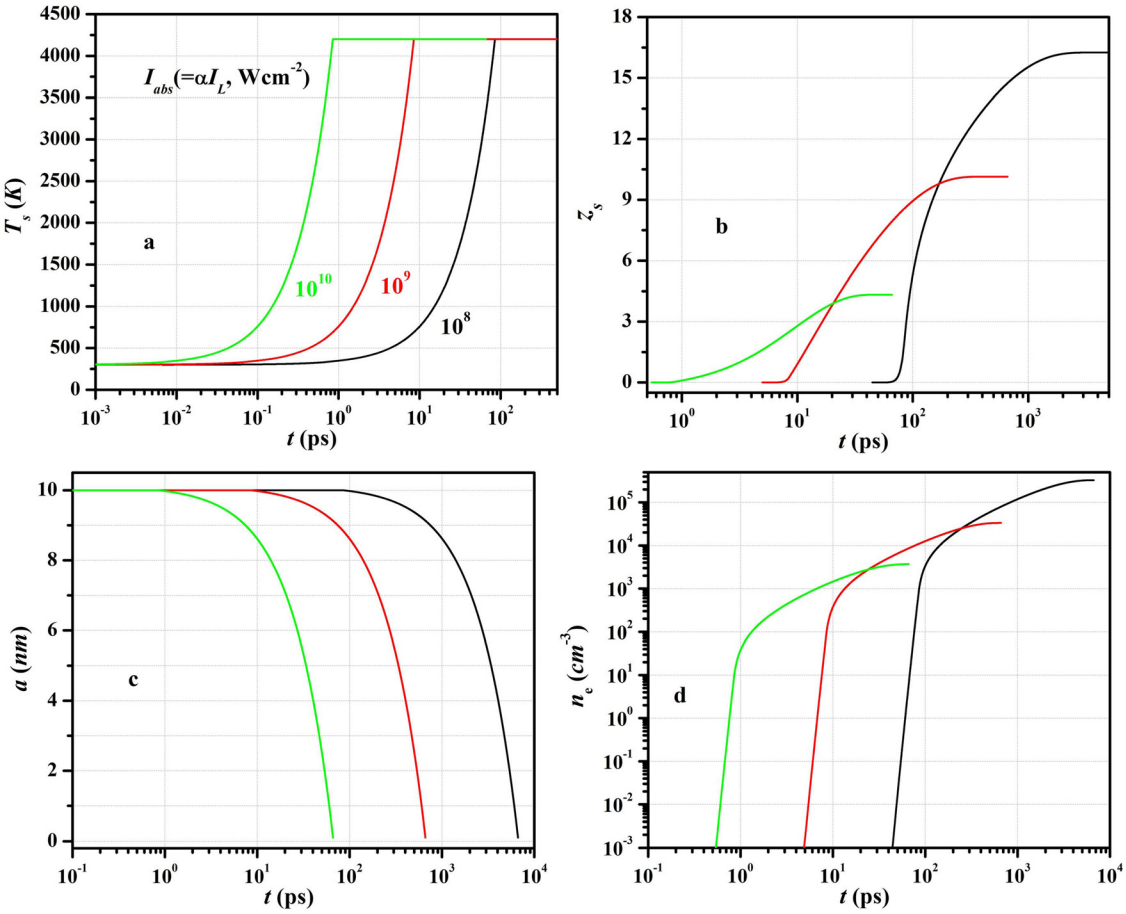

FIG. 2. Transient evolution of nanoparticle (a) temperature (T_s), (b) charge (z_s), (c) radius (a/a_o) and (d) ambient electron density (n_e) for an irradiated graphite nanoparticle cloud. The computations correspond to 300 nm wavelength radiation along with parameters stated in the text and the colour labels in figure refer to different values of radiation flux (I_{abs}).

nanoparticle is not sufficient to overcome van der Waals bonding below the sublimation point (τ_s); this may clearly be observed in Figs. 2(a) and 2(b). In such a case, the charging of nanoparticles is primarily caused by the mass desorption mechanism during material evaporation. The transient evolution of the particle size (a) due to mass desorption is presented in Fig. 2(c). In contrast to Fig. 1(c), τ_s is observed slightly smaller in this case which may be ascribed to the availability of large heat flux ($\gamma = 1$) for the phase change. The electron population density corresponding to 300 nm radiation is displayed in Fig. 2(d), which is qualitatively a manifestation of effects of charging, heating and sublimation processes; a bend in these curves with respect to time refer to an instant where sublimation begins (i.e., τ_s), for instance, for $I_{abs} = 10^8$ W cm^{-2}, the sharp turn occurs at $\tau_s \sim 84.9$ ps. These set of figures (Figs. 1 and 2) specify the effect of radiation on transient evolution of the particle charge, its sustenance at high temperatures and the resulting environment in terms of electron population density. In addition, it also specifies the significance of characteristic timescales associated with disintegration (τ_d), temperature rise to a sublimation point (τ_s) and substance evaporation (τ_a) in describing the typical features of an irradiated nanoparticle cloud.

Concerning the fact that the nanoparticle temperature, charging and evaporation are sensitive to the radiation and material characteristics, the laser/nanoparticle parameters can be tuned such that the nanoparticle cloud may safely operate below the sublimation temperature where the nanoparticles are likely to retain their shape/size; such a parametric regime in terms of radiation intensity and material work function, is presented next. Using the set of kinetic equations [Eqs. (1), (2), (4), and (5)], a set of curves for different values of λ illustrating a relation between radiation flux (I_{abs}) and work function (φ) of the nanoparticle substance such that the data points (φ, $I_{abs} = I_c$) on curve refers to the sublimation temperature of the surface material (graphite in the present case), is demonstrated in Fig. 3(a); the different values of φ considered herein for the parametric study, in a practical situation, may be regarded as contaminated graphite particles. The region (say RI) below the curve corresponds to the parameter regime where nanoparticles sustain below their sublimation point (i.e., $T_s < T_{cr}$, $T_{cr} \sim 4200$ K for graphite[32]) and the particle size remains intact while rest of the area above curve (say RII) refers to the sublimation (phase change) regime. Region RI is observed to decrease with increasing radiation wavelength (or decreasing photon energy). This nature may be understood in terms of spectral dependence of fraction γ of the absorbed energy flux (i.e., γI_{abs}) which is consumed in nanoparticle heating; as the defined γ increases with increasing wavelength and this reduces critical I_{abs} ($\sim I_c$) required to accomplish the sublimation temperature. Similar space has been identified

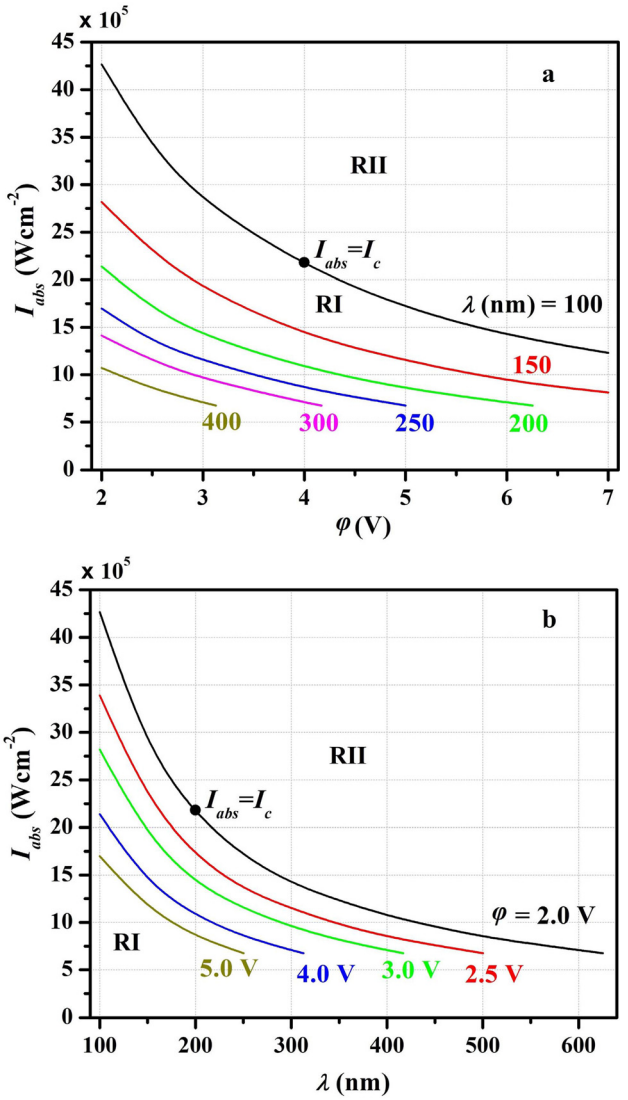

FIG. 3. Parametric space defining sustenance of a laser irradiated nanoparticle below the sublimation point: a relation between (a) radiation intensity (I_{abs}) and material work function (φ) for different wavelength (λ) radiation and (b) radiation intensity (I_{abs}) and radiation wavelength (λ) for different values of material work function (φ); the points on the curve itself refers to the sublimation point, while the area below the curve corresponds to the laser/material parameters where the particles may sustain below sublimation. The computations correspond to the parameters stated in the text and the colour labels in the figure refer to the varying physical parameter.

between the radiation flux (I_{abs}) and the operating wavelength (λ) for different values of material work functions (φ) in Fig. 3(b). Similar to previous case [Fig. 3(a)], the area below the curve (i.e., region RI) describes the flexibility to operate illuminated nanoparticles safely under the sublimation temperature ($T_s < T_{cr}$), while the region RII above the curves correspond to the phase change (mass evaporation) regime. Region RI decreases with increasing work function of the surface material which is primarily a consequence of the availability of a larger photon flux for particle heating; this feature may also apparently be explained on the basis of spectral dependence of γ. The curves terminated at the wavelength/work function equivalent to the respective photoemission threshold. In this set of calculations, we have specified a parametric space in terms of intensity and wavelength/

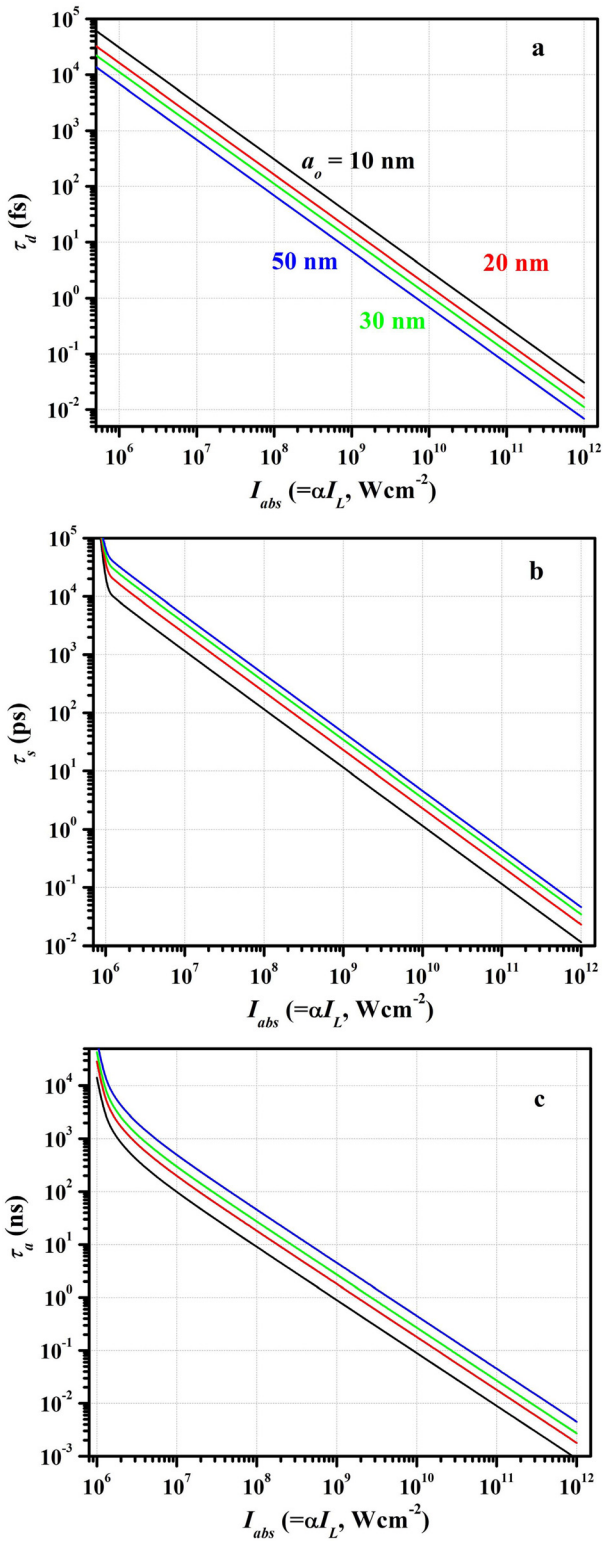

FIG. 4. The characteristic timescales associated with (a) cloud disintegration (τ_d), (b) achieving the sublimation point (τ_s) and (c) substrate evaporation (τ_a) as a function of radiation intensity (I_{abs}) for different values of particle size (a_o). The computations correspond to $\lambda = 200$ nm, $\varphi = 4.6$ V and the parameters stated in text; the colour labels in the figure refer to different values of the varying physical parameter.

material work function where the laser irradiated nanoparticles may safely be operated below critical temperature without sublimation of nanoparticles. It is also noticed that the system operating with the laser wavelength lower than

the photoemission threshold might also avoid the disintegration of the nanoparticle cloud.

As illustrated in earlier discussion, the characteristic times of different phases are crucial in identifying a suitable regime of operation, the dependence of constituent timescales on radiation intensity ($I_{abs} = \alpha I_{in}$) for different size nanoparticles has been illustrated in Fig. 4; the computations correspond to the graphite nanoparticle cloud irradiated by 200 nm wavelength radiation. Since $h\nu > \varphi$, the cloud disintegration is anticipated to occur in the beginning phase of heating i.e., below the sublimation point (refer Fig. 1). The disintegration timescale (τ_d) is observed to decrease with increasing nanoparticle size [Fig. 4(a)]; this nature may be attributed to the particle charge which increases with increasing surface area available for the electron emission. The growth of particle charge increases the Coulomb repulsion between the particles to quickly supersede the van der Waals bonding which brings the disintegration time to a shorter duration. The decay of cloud disintegration time with increasing radiation flux may be interpreted in terms of increasing particle charge with increase in radiation flux through enhanced thermionic/photoemission flux [Fig. 1(a)]. The dependence of the sublimation timescale (τ_s) over the radiation flux and particle size is displayed in Fig. 4(b). The decay in τ_s may be understood in terms of the rate of rise in temperature with increasing radiation flux, while the size dependence may be attributed to the surface cooling through thermionic/photoelectric emission which increases with increasing nanoparticle size/charge [Eq. (2)]. From this figure, it is also evident that below certain intensity, the nanoparticles can sustain for a longer duration; for instance, in this case, the limit is $\sim$0.4 MW cm^{-2}. The timescale associated with complete evaporation (τ_a) has been evaluated as a function of nanoparticle size and incident flux in Fig. 4(c). Obviously a larger size particle, due to large mass desorption in the phase change process, is noticed to evaporate on a longer timescale. The decay with radiation flux is clearly evident from Eq. (5) which reflects that the rate of mass sublimation increases with increasing intensity. Here, we also specify a limit over the radiation intensity (for instance, $\sim$0.4 MW cm^{-2}) below which the evaporation does not take place; it is primarily a consequence of operating the nanoparticle system below the sublimation point.

The effect of varying wavelength (λ) of incident radiation on the characteristic timescales is depicted in Fig. 5; as the observed disintegration time (τ_d) increases with increasing wavelength. This may be understood in terms of decay in photoemission flux from the particle surface due to decreasing photon energy which eventually decreases the particle charge and hence the effective Coulomb repulsion, responsible for the cloud disintegration; this effectively turns out in increasing the disintegration time τ_d. This also signifies the essence of photoemission on nanoparticle charging and cloud disintegration as discussed in Fig. 2. The sublimation time τ_s is noticed to display an opposite trend than τ_d as illustrated in Fig. 5(b); this behaviour may be interpreted through the spectral dependence of energy flux available for nanoparticle heating which increases with increasing wavelength resulting in a quick rise in the surface temperature to acquire the sublimation temperature. The large heat flux access for the phase

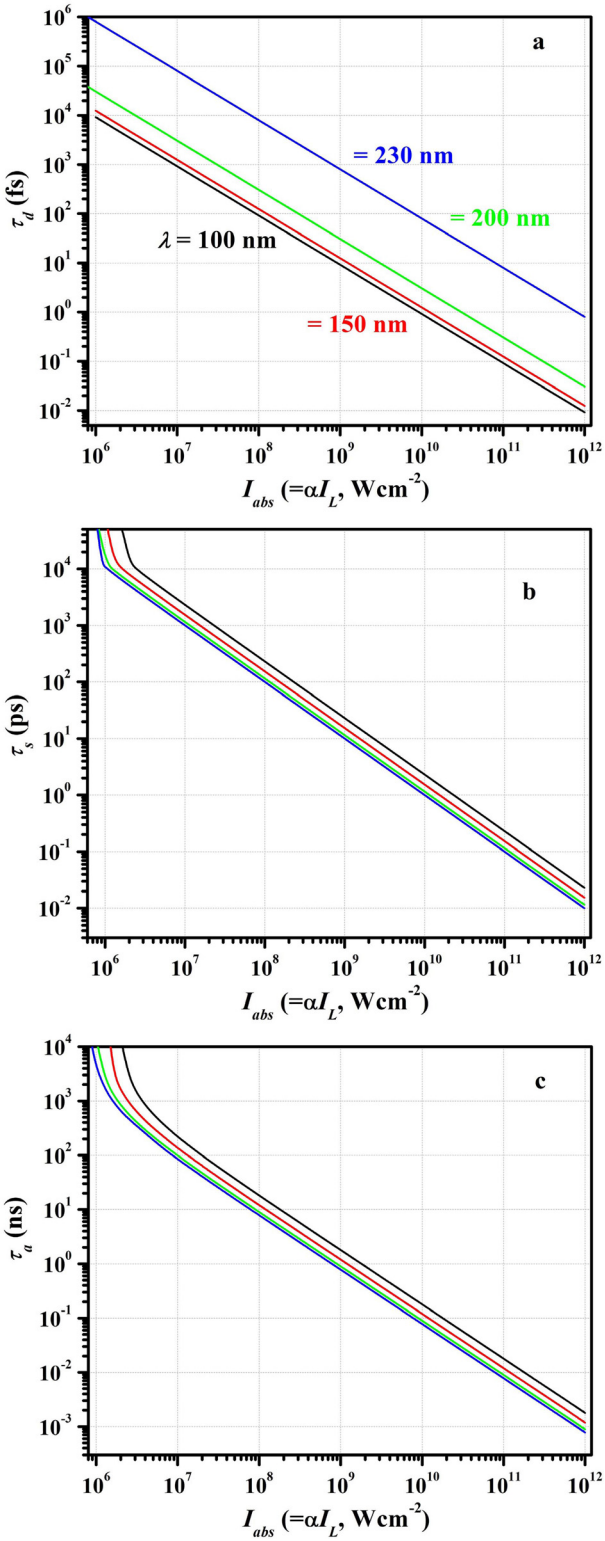

FIG. 5. The characteristic timescales associated with (a) cloud disintegration (τ_d), (b) achieving the sublimation point (τ_s) and (c) substrate evaporation (τ_a) as a function of radiation intensity (I_{abs}) for different values of radiation wavelength (λ). The computations correspond to $a_o = 10$ nm, $\varphi = 4.6$ V and the parameters stated in the text; the colour labels in the figure refer to different values of the varying physical parameter.

change in the case of large wavelength radiation causes faster evaporation of the particle substance through a mass sublimation process resulting in a decrease in evaporation time (τ_a); this nature is illustrated in Fig. 5(c). The figure

also indicates that nanoparticles may sustain for a longer duration without evaporation (i.e., below sublimation) if the radiation flux lies below a certain critical value; for instance, in the case of 100 nm, this critical value refers to $I_{abs} \sim 1.9$ MW cm^{-2} while in the case of 230 nm, it reads ~0.8 MW cm^{-2} below which the particle size remains intact. The influence of varying the work function (φ) of the surface material on the constituent timescales is specified in the set of Fig. 6; the computations have been made with 200 nm wavelength radiation, incident over a cloud of 10 nm graphite nanoparticles. The disintegration time (τ_d) is perceived to increase with increasing work function as illustrated in Fig. 6(a). This behaviour is a consequence of decrease in photoemission flux with increasing φ which ultimately reduces the particle charge; such a decrease in charge relaxes the growth of the Coulomb repulsion in achieving inter-particle bond (van der Waals) energy and hence a larger time span of disintegration (τ_d) is anticipated. The faster rise in the surface temperature (i.e., smaller τ_s) with a smaller work function value may again be understood in terms of γ dependence of threshold radiation (equivalent to φ) which reveals the large heat flux availability for particle heating with increasing φ; this nature is demonstrated in Fig. 6(b). Consequently, the dominant evaporation of particle substance at a shorter timescale (τ_a) with increasing φ may be interpreted which is displayed in Fig. 6(c). The decrease of the constituent timescales with incident radiation flux may be attributed to the rise in surface temperature and consequent charging/heating processes, as discussed earlier. With these estimates of various timescales, one can impose the limitations on the laser pulse duration (τ_o) irradiating the nanoparticle clouds in order to operate the system in different stages. For instance, in reference to a typical case, i.e., a 10 nm graphite nanoparticle cloud irradiated with $I_{abs} = 10^8$ W cm^{-2} (black curve: Fig. 4), the disintegration may be avoided by operating with a pulse <300 fs, while the nanoparticles may sustain below the sublimation point for laser pulses smaller than 115 ps. On the other hand, the particles may completely be vaporized for pulses larger than 10 ns. Thus, one can tune the mode of operation using adequate laser/nanoparticle parameters. It should also be mentioned that although numerical calculations presented herein has been confined to the graphite nanoparticle cloud and particular parameters, the analysis is of general in nature and is applicable to the nanoparticles of any arbitrary substrate with adequate set of parameters. On the basis of numerical calculations, the surface heating, sublimation and nanoparticle cloud disintegration processes are verified to significantly depend on the substrate and radiation specifications. On the basis of present analysis, a reasonable parametric space in terms of radiation intensity/wavelength and material work function describing the laser irradiated nanoparticle ensemble without sublimation (evaporation) has been identified; this estimate gives a flexibility to operate the nanoparticle cloud below the critical sublimation point.

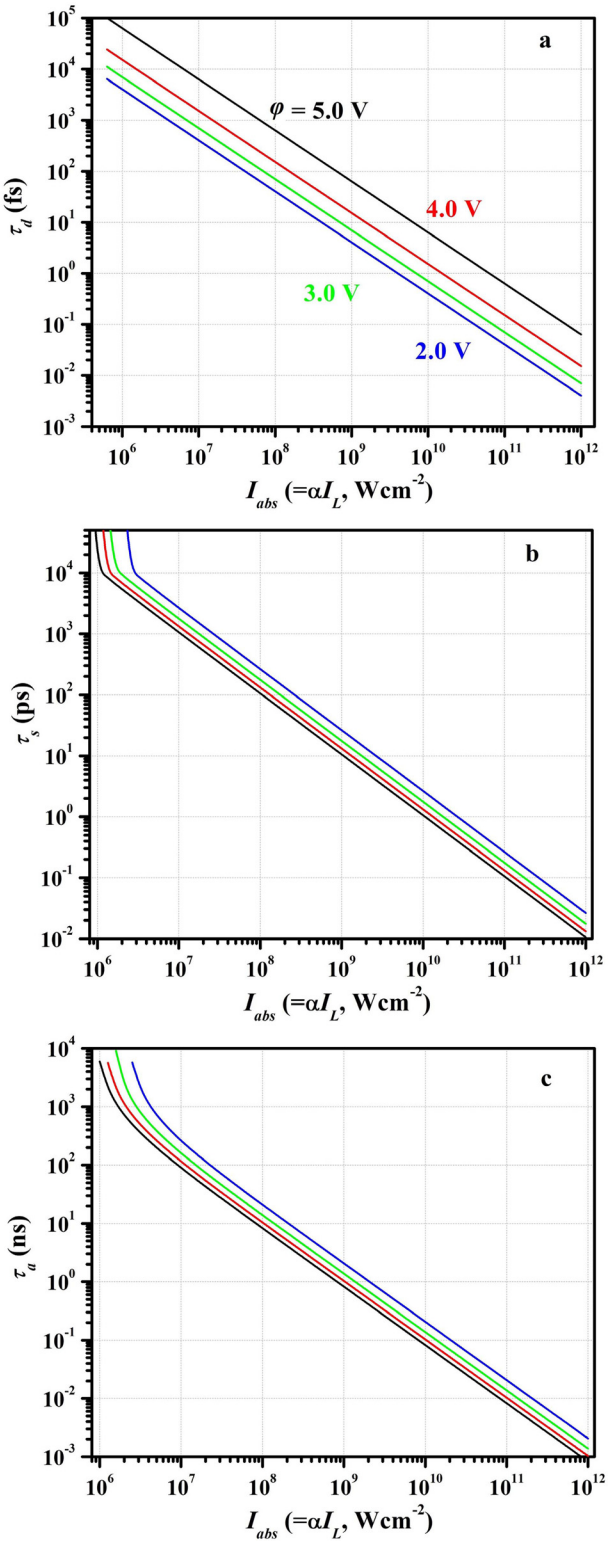

FIG. 6. The characteristic timescales associated with (a) cloud disintegration (τ_d), (b) achieving the sublimation point (τ_s) and (c) substrate evaporation (τ_a) as a function of radiation intensity (I_{abs}) for different values of radiation material work function (φ). The computations correspond to $a_o = 10$ nm, $\lambda = 200$ nm and the parameters stated in the text; the colour labels in the figure refer to different values of the varying physical parameter.

V. SUMMARY AND CONCLUSIONS

A consistent theoretical model describing the complex kinetics of a laser irradiated nanoparticle ensemble has been presented; the formulation takes into account of the electron flux and energy flux balances along with the phase change equation. In contrast to the previous studies,[20,21] a comprehensive analytical model by including the kinetics of

nanoparticle charging, particle heating and material phase change along with the generation and energetics of emitted electrons has been established. Laser illumination of the nanoparticle cloud serves dual purpose, viz., a fraction of absorbed radiation utilized in nanoparticle heating induces thermionic emission of electrons while rest of the proportion is consumed in liberating electrons from the Fermi level through photoemission. In the beginning phase of irradiation, the heating of nanoparticles and a subsequent rise in its temperature are determined through the energy equation [Eq. (2)] which takes account of various heating (laser absorption/electron accretion) and cooling (electron emission/radiation/sublimation) mechanisms, while the nanoparticle charging is governed by continuity of the electron flux [Eq. (1)] via thermionic/photoelectric emission and accretion. The sublimation becomes effective when the surface temperature rises significantly higher than the environment. As soon as the nanoparticle acquires a temperature equivalent to the sublimation (evaporation) point, further rise in temperature ceases and all the energy flux is consumed in the phase change [Eq. (3)] resulting in mass desorption. This ultimately causes the decay in nanoparticle mass/radius, and the nanoparticle charging via material desorption becomes significant. Through transient analysis, nanoparticle charging, surface temperature, mass desorption (i.e., particle size reduction) and ambient electron density have been numerically investigated. In this course, the characteristic timescales referring to the phenomena of cloud disintegration, temperature rise to the sublimation point and substrate evaporation have been identified which are found to be sensitive to radiation and material properties. The estimates of the timescales presented herein also put a constraint on the pulse duration in order to operate the irradiated nanoparticle cloud in different kinetic phases. The cloud disintegration is found to be fairly sensitive to the photoelectric charging of the nanoparticles as it occurs in the beginning and evaporation phases of the process for the radiation operation, respectively, above and below the photoemission threshold. Utilizing numerical analysis in reference to the graphite nanoparticle cloud, a parametric space in terms of radiation flux, wavelength and material work function has been identified where the irradiated nanoparticles sustain below the sublimation temperature without substrate evaporation. Though the numerical results are devoted to the graphite nanoparticle cloud, the analysis is well applicable to any arbitrary substrates with known physical parameters. The analysis, in general, aids the physics understanding of photo-thermal effects from the nanoparticle ensemble under various physical conditions.

As the analysis takes account of few simplifications in modelling, it is of essence to point out its applicability; here, we discuss the limitations of the present analysis and consequent predictions. As a simplification, the analysis is limited to the spherical shape of the nanoparticles. In practice, the nanoparticle shape may be irregular (non-spherical) and the mass sublimation may be inhomogeneous; intuitively, such particles lost for longer than that of the usual spherical case.[26] In order to minimize the computational complexity, cloud irradiation through a monochromatic source causing photoemission from nanoparticles has been considered a simplification; the broader/continuous pulse spectrum[23,24] may effectively be included by integrating the constituent electron emission flux over the radiation spectrum. As another simplification, the nanoparticles in the cloud are considered to be connected through van der Waals bonds, which is a practical situation for less amorphous nanoparticles (like fullerene[34] and metal oxides[35]); however, in the case of a combustion generated soot cloud, the nanoparticles may interact through covalent/chemical bonding.[36] Furthermore, as mentioned earlier, the analysis takes account of the mean charge theory, and energy equations are written in terms of particle surface area; the results corresponding to an individual nanoparticle (namely a, T_s, z_s and the constituent time scales τ_d, τ_s, τ_a) are equally applicable for all the nanoparticles in the cloud, provided the nanoparticles are uniformly irradiated (irrespective of the cloud size). However, it is important to note that in a realistic scenario, there are many effects[20] in the heating and sublimation phases like electron attachment processes to the gas molecules, oxidation of nanoparticles, mutual interaction between particles in the combustion phase and nanoparticle dynamics itself which has not been incorporated in this analysis, due to which the cloud size may be of significance. These features are not in the scope of present work, but would certainly be of concern in future investigations. Another concern may be the choice of an adequate phase diagram which has been taken to be specified via the Clausius-Clapeyron relation as a simplified expression in defining the sublimation rate; this feature should specifically be identified for the system/experimental parameters to be taken into consideration. These aforementioned aspects certainly limit the applicability of the present results, but, of course, the model gives an approximate solution/scaling describing the kinetic features of a laser irradiated nanoparticle ensemble and put forward a basis for further advancement.

ACKNOWLEDGMENTS

This work was performed under the ELI-ALPS project (GINOP-2.3.6-15-2015-00001) which was supported by the European Union and co-financed by the European Regional Development Fund.

[1]K. E. Mueggenburg, X.-M. Lin, R. H. Goldsmith, and H. M. Jaeger, Nat. Mater. **6**, 656 (2007).
[2]A. Tao, P. Sinsermsuksakul, and P. Yang, Nat. Nanotechnol. **2**, 435 (2007).
[3]S. Acharya, J. P. Hill, and K. Ariga, Adv. Mater. **21**, 2959 (2009).
[4]S. Liu and Z. Tang, J. Mater. Chem. **20**, 24 (2010).
[5]Y. Yamada, C.-K. Tsung, W. Huang, Z. Huo, S. E. Habas, T. Soejima, C. E. Aliaga, G. A. Somorjai, and P. Yang, Nat. Chem. **3**, 372 (2011).
[6]T. Wen, R. A. Booth, and S. A. Majetich, Nano. Lett. **12**, 5873 (2012).
[7]A. Manjavacas, J. G. Liu, V. Kulkarni, and P. Nordlander, ACS Nano **8**, 7630 (2014).
[8]K. Yamada, K. Miyajima, and F. Mafuné, J. Phys. Chem. C **111**, 11246 (2007).
[9]M. Valenti, A. Venugopal, D. Tordera, M. P. Jonsson, G. Biskos, A. Schmidt-Ott, and W. A. Smith, ACS Photonics **4**, 1146 (2017).
[10]T. A. Sipkens and K. J. Daun, Opt. Express **25**, 5684 (2017).
[11]H. A. Michelsen, C. Schulz, G. J. Smallwood, and S. Will, Prog. Energy Combust. Sci. **51**, 2 (2015).

[12]C. Schulz, B. F. Kock, M. Hofmann, H. Michelsen, S. Will, B. Bougie, R. Suntz, and G. Smallwood, Appl. Phys. B **83**, 333 (2006).
[13]A. Eremin, E. Gurentsov, and C. Schulz, J. Phys. D: Appl. Phys. **41**, 055203 (2008).
[14]F. Cignoli, C. Bellomunno, S. Maffi, and G. Zizak, Appl. Phys. B **96**, 593 (2009).
[15]T. A. Sipkens, N. R. Singh, and K. J. Daun, Appl. Phys. B **123**, 14 (2017).
[16]G. Gonzalez-Rubio, A. Guerrero-Martinez, and L. M. Liz-Marzan, Acc. Chem. Res. **49**, 678 (2016).
[17]S. K. Mishra, K. Avinash, and P. K. Kaw, J. Plasma Phys. **80**, 863 (2014).
[18]S. K. Mishra, S. Misra, and M. S. Sodha, Plasma Phys. Controlled Fusion **56**, 055005 (2014).
[19]H. Michelsen, F. Liu, B. F. Kock, H. Bladh, A. Boiarciuc, M. Charwath, T. Dreier, R. Hadef, M. Hofmann, J. Reimann, S. Will, P. Bengtsson, H. Bockhorn, F. Foucher, K. Geigle, C. Mounaim-Rousselle, C. Schulz, R. Stirn, B. Tribalet, and R. Suntz, Appl. Phys. B **87**, 503 (2007).
[20]J. M. Mitrani, M. N. Shneider, B. C. Stratton, and Y. Raitses, Appl. Phys. Lett. **108**, 054101 (2016).
[21]L. Zhou, K. Park, H. M. Milchberg, and M. R. Zachariah, Aerosol Sci. Technol. **41**, 818 (2007).
[22]A. Filippov, M. Markus, and P. Roth, J. Aerosol Sci. **30**, 71 (1999).
[23]M. S. Sodha, S. Misra, and S. K. Mishra, Phys. Plasmas **16**, 123705 (2009).
[24]M. S. Sodha, *Kinetics of Complex Plasmas* (Springer, New Delhi, 2014).
[25]M. Massicotte, P. Schmidt, F. Vialla, K. Watanabe, T. Taniguchi, K. J. Tielrooij, and F. H. L. Koppens, Nat. Commun. **7**, 12174 (2016).
[26]D. A. Mendis, W. H. Wong, M. Rosenberg, and G. Sorasio, J. Atmos. Terr. Phys. **67**, 1178 (2005).
[27]S. Misra and S. K. Mishra, MNRAS **459**, 2486 (2016).
[28]R. H. Fowler, *Statistical Mechanics: The Theory of the Properties of Matter in Equilibrium* (Cambridge University Press, London, 1955).
[29]M. U. Kahaly, S. Misra, and S. K. Mishra, J. Appl. Phys. **121**, 205110 (2017).
[30]G. Briani, E. Pace, S. N. Shore, G. Pupillo, A. Passaro, and S. Aiello, Astron. Astrophys. **552**, A53 (2013).
[31]H. Hamaker, Physica **4**, 1058 (1937).
[32]F. O. Goodman and N. Garcia, Phys. Rev. B **43**, 4728 (1991).
[33]D. R. Lide, *CRC Handbook of Chemistry and Physics*, 85th ed. (Taylor & Francis Group, New York, 2004).
[34]J. L. Atwood, L. J. Barbour, M. W. Heaven, and C. L. Raston, Angew. Chem. **115**, 3376 (2003).
[35]Y. Lalatonne, J. Richardi, and M. Pileni, Nat. Mater. **3**, 121 (2004).
[36]H. A. Michelsen, A. V. Tivanski, M. K. Gilles, L. H. van Poppel, M. A. Dansson, and P. R. Buseck, Appl. Opt. **46**, 959 (2007).